Integration of Gas Sensors with CMOS Technology

Lado Filipovic
Institute for Microelectronics, TU Wien
1040 Wien, Austria
filipovic@iue.tuwien.ac.at

Siegfried Selberherr
Institute for Microelectronics, TU Wien
1040 Wien, Austria
selberherr@iue.tuwien.ac.at

***Abstract*—For the last several decades, the primary concern of the semiconductor industry was transistor scaling along Moores Law. However, as scaling on silicon approaches its physical limits, several research avenues have been directed towards functional integration of different devices using the More-than-Moore approach. The main goal of this approach is the integration of sensors, RF circuits, and other functionalities in CMOS technology in order to enable non-digital system-in-package and digital system-on-chip integration for a higher value system. This can be achieved by innovation in packaging, three-dimensional integration, and fabrication using mature CMOS technology on silicon. When it comes to gas sensors, semiconductor metal oxide (SMO) thin film based sensors have recently shown their potential for integration with digital electronics, which is an important step to their integration in wearable and portable electronics. The recent achievements in the integration of SMO sensors with CMOS fabrication are very promising. The complexity therein lies in the need for an integrated microheater, since SMO films operate as sensors only at quite high temperature. The microheater, therefore, must be isolated from other electronics, which is achieved by using a suspended membrane with an air cavity underneath, a feature common in microelectromechanical systems (MEMS). The power- and performance-optimized integration of MEMS and CMOS requires many design trade-offs. Among recent achievements is the fabrication of perforated membranes, which combine the benefits of their suspended and closed alternatives. Finally, several outstanding concerns which are still hindering a full integration of SMO sensors in wearable and hand-held electronics are described and current approaches to engineer solutions are summarized.**

***Index Terms*—gas sensors, semiconductor metal oxide, modeling and simulation, perforated membrane, MEMS microheater**

I. Introduction

Our perception of the environment is greatly influenced by the molecular composition of the gases in our vicinity. Our nose is very efficient in detecting a broad variety of different smells, but it is unable to pinpoint exact gas concentrations and can fail entirely in the detection of several highly poisonous gases, such as carbon monoxide (CO). Many gases are only harmful above a certain concentration, which is why many governments and organizations put regulations and limit the amount of these pollutants in order to reduce risks to humans and the environment. The different standards used for the World Health Organization (WHO), the United States Environmental Protection Agency (EPA), and the European Commission (EC) are given in Table I [1], where in particular the harmful concentration standards of common pollutants, including CO, nitrogen dioxide (NO_2), ozone (O_3), sulfur dioxide (SO_3), particulate matter ($PM_{2.5}$ and PM_{10}), and lead (Pb) are summarized. It is clear that industry requires sensors to detect a broad range of pollutants at varying concentrations. Gas detection has been a topic of interest for decades, and prior to the advent of gas sensors, animals were primarily used for sensing of certain gases. A prototypical example is the use of a canary for gas detection in mines, as it stops singing once exposed to methane, CO, or carbon dioxide.

TABLE I
Different standards of some common pollutants from [1]

Pollutant	WHO	EPA	EC
CO	10 mg/m^3 (8h) 15 mg/m^3 (1h)	9ppm (8h) 35ppm (1h)	10 mg/m^3 (8h)
NO_2	200 μg/m^3 (1h) 40 μg/m^3 (1yr)	100 ppb (1h) 53 ppb (1yr)	200 μg/m^3 (1h) 40 μg/m^3 (1yr)
O_3	100 μg/m^3 (8h)	75 ppb (8h)	120 μg/m^3 (8h)
SO_2	500 μg/m^3 (10min) 20 μg/m^3 (24h)	75 ppb (1h) 0.5 ppm (3h)	350 μg/m^3 (1h) 125 μg/m^3 (24h)
$PM_{2.5}$	25 μg/m^3 (24h) 10 μg/m^3 (1yr)	35 μg/m^3 (24h) 12 μg/m^3 (1yr)	25 μg/m^3 (1yr)
PM_{10}	50 μg/m^3 (24h) 20 μg/m^3 (1yr)	150 μg/m^3 (3mth)	50 μg/m^3 (24h) 40 μg/m^3 (1yr)
Pb	0.15 μg/m^3 (3mth)	0.5 μg/m^3 (1yr)	0.5 μg/m^3 (1yr)

The development and advancement of gas sensors is of interest in many industries, including health and safety [2], environmental monitoring [3], automotive [4], and chemical warfare detection [5]. One of the primary goals of researchers in the gas sensor field is allowing for its miniaturization and reducing its power consumption in order to allow for its integration into portable and wearable electronics.

Aggressive transistor scaling along Moore's Law [6] has enabled today's hand-held and wearable devices, powered by advancements in CMOS fabrication technology. However, recently, there has been growing interest in the integration of multiple applications, such as sensors, radio frequency (RF) circuits, on a single chip, labeled the More-than-Moore approach [7]. The integration of micro-electro-mechanical systems (MEMS), such as sensors, with CMOS technology can be achieved using three-dimensional (3D) integration. This technique allows for die stacking, thereby eliminating the need for long bonding wires and enabling a straightforward single packaging step. The ideal integration between MEMS and CMOS rests on having all necessary features and devices fabricated using CMOS technology with materials and techniques readily available in a CMOS fabrication facility, all on a single wafer. By fabricating the electronics and MEMS features on the same wafer, enabling fast interconnections between different circuits required by a complete internet of things sensor or integrated sensor system becomes intuitive.

In this review the achievements made in the integration of gas sensors with CMOS technology are discussed. This is pri-

978-1-7281-2539-8/20/$31.00 ©2020 IEEE 2020 IEEE Electron Devices Technology and Manufacturing Conference Proceedings of Technical Papers

marily relevant for the semiconductor metal oxide (SMO) gas sensor, whose fabrication is integrable with CMOS fabrication. Achievements made in the design and fabrication of SMO sensors are further discussed. The primary concern therein is the integration of a microheater, required to heat the sensing film to several hundred degrees Celsius to enable efficient sensing. Before discussing the SMO sensor, different gas sensing mechanisms are described in the subsequent section.

II. Gas Sensors

Many different types of gas sensors are currently being investigated at different levels of development. Many sensors and potential sensing films are still at the research infancy phase, including two-dimensional (2D) semiconductors such as graphene and transition metal dichalcogenides (TMDs) [8]. The fabrication and synthesis of these films is not trivial and research on how to obtain high quality thin films consistently is still out of our reach. In this section the currently available mature technologies for gas detection are described and their advantages and disadvantages are discussed.

A. Gas Sensing Mechanisms

A variety of mature gas sensing technologies are currently implemented in industry, including semiconductor, catalytic pellistors (CP), piezo-electric (PE), electro-chemical (EC), thermal pellistor (TP), photo-ionization (PI), and infrared (IR) adsorption [9], [10], [11], [12], [13], whose properties are summarized in Table II. These sensors are classified into two groups, those whose sensing is based on a change in a material's electrical properties and those whose sensing is based on changes in other properties [14].

From Table II the SMO sensor has the highest power, cost, and footprint ratings, owing to its integration with CMOS technology. These three components are essential for portability applications and integration. CMOS technology integration also allows for excellent reproducibility and repeatability [15]. It is of critical importance that the same structure with a predictable geometry and predictable operating conditions is fabricated with well controlled tolerances, when developing commercial devices. While the catalytic pellistor also enjoys low power consumption, cost, and a relatively small footprint, its selectivity is very poor, while its sensitivity is weaker and response time is longer than that of an SMO sensor. The piezo-electric sensor, on the other hand, has an excellent sensitivity, accuracy, and response time, but its power consumption is a limitation to portability. The same can be said for the photo-ionization and IR adsorption sensors. The electro-chemical sensor requires a large footprint, while the sensitivity of a thermal pellistor is not up to par with an SMO sensor. All in all, the SMO sensor provides the most advantages over alternatives, especially, when it comes to its sensitivity, response time, and potential for miniaturization and portability through very low power consumption, very low fabrication costs, and a very small footprint.

B. SMO Gas Sensors

Recent investigations into SMO films have been geared towards enhancing gas sensor sensitivity and selectivity by testing a multitude of SMO films and designing novel composite materials. Some films which have been tested recently include ZnO, SnO_2, α-Fe_2O_3, CdO, $ZnSnO_4$, NiO, PbO, YSZ, WO_3, ITO, and In_2O_3 [16], [17]. From the SMOs studied, SnO_2, which is an n-type wide band-gap semiconductor, appears to have the most relevant properties, including a high electron mobility (160cm^2/V·s) and a high chemical and thermal stability [17]. SnO_2 was also shown to be highly sensitive towards many gases and its deposition can be incorporated into CMOS technology using spray pyrolysis. For these reasons, SnO_2 has recently been commercialized by several vendors [13].

TABLE II
Advantages and disadvantages of available gas sensing technologies. 4=Excellent, 3=Good, 2=Fair, 1=Poor.

Parameter	SMO	CP	PE	EC	TP	PI	IR
Sensitivity	4	3	4	3	1	4	4
Accuracy	3	3	4	3	3	4	4
Selectivity	2	1	2	3	1	2	4
Speed	4	3	4	2	3	4	2
Stability	3	3	3	1	3	4	3
Durability	3	3	2	2	3	4	4
Power	4	4	2	3	3	1	2
Cost	4	4	3	3	3	2	2
Footprint	4	3	3	2	3	4	1

The sensing mechanism of SMO films is based on molecular chemisorption of a gas molecule on the surface of an SMO film, when the film is heated to elevated temperatures (250°C - 550°C). The need for high temperature operation demands the integration of a microheater, where the high temperature components must be isolated from the other circuit components. For this purpose, a MEMS membrane, which is suspended in air, is commonly used, depicted in Fig. 1.

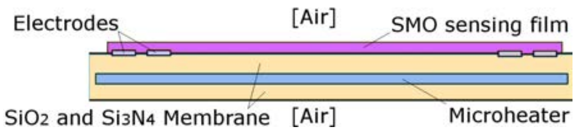

Fig. 1. SMO sensor membrane stack, depicting the membrane layer (SiO_2/Si_3N_4), the microheater, the electrodes, and the SMO sensing film.

The molecular adsorption causes charge accumulation and a subsequent change in the resistance of the film. In the case of a granular film, the surface of each grain can serve as an adsorption site. With this fact in mind, it immediately becomes clear, why selectivity is an issue, as there is no direct way for the film to know which molecule caused the charge accumulation on the surface. The selectivity can, however, be implemented artificially by introducing a sensor array, where multiple sensing films are used to simultaneously sense the ambient [18], [19], [20], [21], [22], [23]. One alternative is to have the same sensing film, but using different dopants at different sensing sites. Another option is to operate different locations of the sensing film at different temperatures, each optimized for a particular gas molecule. The collected data can subsequently be processed with a variety of methods such as neural networks [23] or machine learning algorithms [24].

C. Surface Adsorption

The conduction of the SnO_2 film is modeled using drift-diffusion equations [25], commonly used to describe charge

transport in semiconductors [26]. Since the thicknesses of the SMO layers applied in gas sensors are comparable to the mean free path of the charge carriers, the diffusion component can be ignored and the conductivity becomes $\sigma = q \cdot n \cdot \mu_n$, with q the electron charge, n the electron concentration, and μ_n the electron mobility. The sensitivity of a resistive gas sensor relies on its surface-to-volume ratio, since sensing is the change in a volume behavior (resistance) due to a surface event (adsorption). The porous SMO sensing film contains many grains and on the surface of those grains, adsorption takes place. The bulk conductivity is determined by the electron transport through the grain-grain, grain-bulk, and grain-electrode interfaces [27]. Since the charge mobility does not change during molecular adsorption, the sensing mechanism depends on increasing or decreasing surface charge concentrations [28].

The steps in the sensing of a gas (e.g., CO) on SnO_2 is depicted in Fig. 2 and starts by surface oxygen ionosorption, which takes one (O^-) or two (O^{-2}) electrons from the bulk, respectively, thereby creating a depletion region around the grain (Fig. 2a). In the presence of CO gas, CO molecules react with adsorbed oxygen, releasing the electron to the bulk, reducing the thickness of the depletion region, and releasing CO_2 gas (Fig. 2b) [27], [28]. It was recently found that, even without oxygen, CO can adsorb on the SnO_2 surface, donating an electron and forming an accumulation region (Fig. 2c) [29].

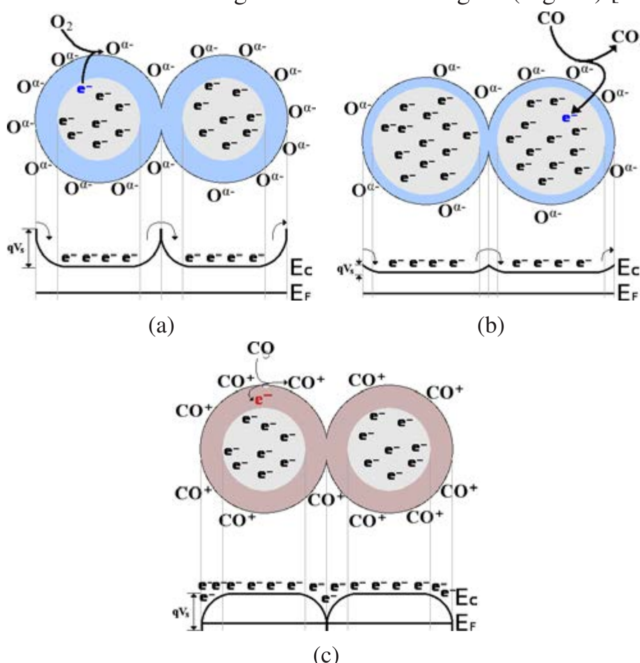

Fig. 2. Surface adsorption of CO on granular SnO_2. (a) Oxygen adsorbs on the surface, forming a depletion region, (b) CO reacts with oxygen, reducing the depletion region and releasing CO_2 gas, and (c) after oxygen depletion, CO adsorbs on the surface, forming an accumulation region.

The influence of noble metal additives on SMO films has also been readily studied [17], [30], from which several conclusions have been drawn: The addition of noble metal additives improves the sensor response, but a shift in the optimal operating temperature is noted, especially with Pt doping [30]. Furthermore, doping with metal additives can over-saturate the sensor performance (e.g., 0.5 mol% Rh performs better than 1.0 mol% Rh SnO_2) [17]. A similar phenomenon was observed in studies of Pt-doped SnO_2 [31]. One reason for this phenomenon can be attributed to the *localized* consumption of gas molecules by Pt without additional electron transfer, which does not result in changes of the SnO_2 film's resistivity.

III. SMO Sensor Design and Fabrication

Fabricating the SMO sensor requires several critical processing steps. The most challenging of which for CMOS integration is the membrane release, or the creation of a void under the membrane which houses the microheater (Fig. 1) [32]. It should be noted that sensor design and optimization relies greatly on electro-thermo-mechanical simulations (e.g., using finite element methods) prior to fabrication and testing [13], [33]. Attempting novel and innovative designs and materials in a laboratory requires a long time and costly equipment which can increase design costs tremendously. However, gas sensors still require calibration and optimization before full integration. For this purpose, simulations are essential when attempting novel and innovative designs, in order to avoid the costs and time associated with laboratory experimentation.

A. Membrane Release

Three primary membrane types have been investigated for SMO gas sensors, including suspended [34], closed [35], and perforated [36] ones. The fabrication steps required to fabricate such membranes are outlined in Fig. 3. The suspended membrane is formed by patterning the suspension beams using photolithography and front-side wet chemical etching (e.g., KOH or TMAH) or using selective plasma etching, which is a CMOS compatible process [37]. The suspended membranes are generally very thin and the process is CMOS compatible, but care must be taken to ensure that the highly reactive wet chemical etchant does not damage other sections of the wafer.

The closed membrane is fabricated by forming the membrane on the front-side of the wafer and etching to it from the back of the wafer (Fig. 3c) using wet chemical etching or deep reactive ion etching (DRIE), which is a cyclical etching process, where each cycle consists of isotropic deposition of a fluorocarbon polymer followed by ion-enhanced etching in a reactive plasma [33], [38]. The key advantage of the closed membrane is its mechanical stability, but this comes at a price of higher power dissipation, since more of the membrane is attached to the die, resulting in higher heat conduction [39].

The perforated membrane combines the advantages of the suspended and closed membrane types. It uses a sacrificial layer and is etched form the front-side (Fig. 3b), meaning that the membrane can be as thin as the suspended variant. The membrane is released by introducing a sacrificial polyimide, depositing a membrane on top of it, etching holes in that membrane, then selectively etching away the polyimide through those holes [36], [40]. The holes also allow to reduce the lateral heat conduction and heat losses through the membrane, reducing the total power consumption and mechanical strain.

B. Microheater Design

Since the key requirement for microheater materials is to be susceptible to Joule heating, a broad variety of materials

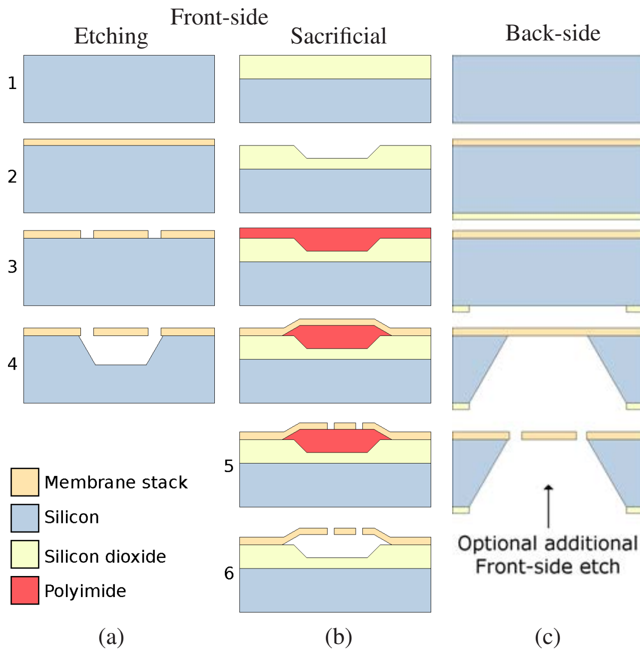

Fig. 3. Etching steps used to release the SMO sensor membrane. (a) Front side etching for a suspended membrane. (b) Sacrificial Polyimide etching for a perforated membrane. (c) Back-side etching for a closed membrane.

have the potential for this function. Materials such as silicon carbide (SiC), polysilicon (poly-Si), aluminum (Al), copper (Cu), molybdenum (Mb), platinum (Pt), tungsten (W), nickel alloys, tantalum-aluminum (TaAl), and many others have been used to heat the SMO sensing film [41]. While SiC has very high potential, its use strays from silicon-based membrane stacks and is not compatible with CMOS technology. Initially Al and poly-Si, materials, readily available in CMOS foundries, were used as microheaters [42]. However, these suffer from electromigration and have poor contact properties at high temperatures, which is why today Pt is very commonly used [41], [43]. Pt is nevertheless not ideal due to its high cost and its positive temperature coefficient of resistance (TCR), resulting in increased hotspot effects, leading to drift in the sensor response and poor long-term reliability [44]. Several other materials have recently been tested with varying success, including W [35], TaAl [40], and Mb [45]. A good microheater material provides a low thermal conductivity, high electrical resistivity, high melting point, low CTE, low Poisson's ratio, and high compatibility with CMOS technology [43].

In order to improve the temperature uniformity over the active sensor area, many innovative microheater designs have been investigated [12]. Most commonly, variations of the meander and circular designs have been applied in today's devices as shown in Fig. 4. In order to further improve temperature uniformity, many researchers also introduce an electrically inert, but highly thermally conductive plate in the membrane stack below or above the microheater [33].

IV. Conclusion and Outlook

Great strides have recently been made in the SMO sensor integration with CMOS technology. Among them is the fabrication of perforated membranes, which provides combined benefits of the suspended membrane (thin and low power consumption) and the closed membrane (mechanical stability). However, several improvements for the fabrication and design of SMO sensors are still desired for full integration with CMOS technology and portable electronics, including:

- Reduce the operating temperature to lower the power consumption and improve the mechanical stability of the sensor.
- SMO sensor simulation and design tools which include the influence of the microheater's temperature non-uniformity.
- Replacing the sensor array, needed for selectivity, with power efficient alternatives, such as a microheater array.
- While adsorption is somewhat understood, it is unclear how to ensure desorption of gas molecules after a sensing event, especially in portable electronics [46]. Ideally, returning to room temperature should result in desorption, but this is not the case and a removal procedure must be incorporated.

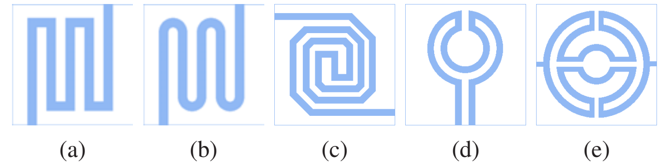

Fig. 4. Commonly used microheater designs, including (a) meander, (b) curved, (c) double spiral, (d) circular, and (e) drive-wheel geometries.

References

[1] W. Y. Yi *et al.*, *Sensors* **15**(12) pp. 31 392–31 427, 2015.
[2] H. Li *et al.*, *IEEE Sensors J* **14**(10) pp. 3391–3399, 2014.
[3] G. F. Fine *et al.*, *Sensors* **10**(6) pp. 5469–5502, 2010.
[4] R. Moos *et al.*, *Sens Actuators B* **83**(1-3) pp. 181–189, 2002.
[5] R. Yoo *et al.*, *Sens Actuators B* **221** pp. 217–223, 2015.
[6] G. E. Moore, *Electronics* **38**(8) pp.114–117, 1965.
[7] W. Arden *et al.*, "More-than-Moore white paper," 2010.
[8] R. Ghosh *et al.*, *IEEE Trans Electron Devices* **66**(8) pp. 3254–3264, 2019.
[9] G. Eranna *et al.*, *Crit Rev Solid State* **29**(3-4) pp. 111–188, 2004.
[10] G. Korotcenkov, *Mat Sci Eng B-Adv* **139**(1) pp. 1–23, 2007.
[11] A. Dey, *Mat Sci Eng B-Adv* **229** pp. 206–217, 2018.
[12] L. Filipovic and A. Lahlalia, *J Electrochem Soc* **165**(16) pp. B862–B879, 2018.
[13] L. Filipovic and S. Selberherr, *Materials* **12**(15) p. 2410, 2019.
[14] X. Liu *et al.*, *Sensors* **12**(7) pp. 9635–9665, 2012.
[15] A. Ponzoni *et al.*, *Sensors* **17**(4) p. 714, 2017.
[16] L. Filipovic and S. Selberherr, *Sensors* **15**(4) pp. 7206–7227, 2015.
[17] X. Kou *et al.*, *Sens Actuators B* **256** pp. 861–869, 2018.
[18] B. T. Marquis and J. F. Vetelino, *Sens Actuators B* **77**(1-2) pp. 100–110, 2001.
[19] N. Barsan *et al.*, *Sens Actuators B* **121**(1) pp. 18–35, 2007.
[20] K. T. Ng *et al.*, *IEEE Trans Circuits Syst* **58**(7) pp. 1569–1580, 2011.
[21] T. Konduru *et al.*, *Sensors* **15**(1) pp. 1252–1273, 2015.
[22] L. A. Horsfall *et al.*, *J Mater Chem A* **5**(5) pp. 2172–2179, 2017.
[23] D. Zhang *et al.*, *Sens Actuators B* **240** pp. 55–65, 2017.
[24] Y.-H. Liao *et al.*, *Sensors* **19**(8) p. 1866(15), 2019.
[25] G. Tulzer *et al.*, *Nanotechnology* **24**(31) p. 315501(10), 2013.
[26] L. A. Caffarelli and A. Vasseur, *Ann Math* **171** pp. 1903–1930, 2010.
[27] N. Barsan and U. Weimar, *J Electroceramics* **7**(3) pp. 143–167, 2001.
[28] D. Degler *et al.*, *J Mater Chem A* **6**(5) pp. 2034–2046, 2018.
[29] N. Bârsan *et al.*, *Sens Actuators B* **157**(2) pp. 510–517, 2011.
[30] M. Saberi *et al.*, *Sens Actuators B* **206** pp. 617–623, 2015.
[31] L. Mädler *et al.*, *J. Nanoparticle Res* **8**(6) pp. 783–796, 2006.
[32] E. Lackner *et al.*, *Mater Today* **4**(7) pp. 7128–7131, 2017.
[33] R. Coppeta *et al.*, "Electro-thermal-mechanical modeling of gas sensor hotplates," in *Sensor Systems Simulations*, W. D. van Driel *et al.*, Eds. Springer Nature Switzerland AG, 2020; Chapter 2, pp. 17–72.
[34] A. Lahlalia *et al.*, *IEEE Sensors J* **18**(5) pp. 1960–1970, 2018.
[35] S. Z. Ali *et al.*, *IEEE Sensors J* **15**(12) pp. 6775–6782, 2015.
[36] A. Lahlalia *et al.*, *Sensors* **19**(2) p. 374(14), 2019.
[37] C. Dücsö *et al.*, *Sens Actuators A* **60**(1-3) pp. 235–239, 1997.
[38] F. Lärmer and A. Urban, *Microelectron Eng* **67** pp. 349–355, 2003.
[39] A. I. Uddin *et al.*, *Sens Actuators B* **207** pp. 362–369, 2015.
[40] A. Lahlalia *et al.*, *J Microelectromech S* **27**(3) pp. 529–537, 2018.
[41] L. Filipovic and S. Selberherr, "CMOS-compatible gas sensors," in *Proc. MIEL*, 2019 pp. 9–16.
[42] K. Zhang *et al.*, *Int J Therm Sci* **46**(6) pp. 580–588, 2007.
[43] I. Simon *et al.*, *Sens Actuators B* **73**(1) pp. 1–26, 2001.
[44] L. Xu *et al.*, *IEEE Sensors J* **11**(4) pp. 913–919, 2010.
[45] L. L. R. Rao *et al.*, *IEEE Sensors J* **17**(1) pp. 22–29, 2016.
[46] S. Woo Lee *et al.*, *Sens Actuators B* **41**(1-3) pp. 55–61, 1997.